Lactate regulates osteoclastogenesis via H3K18la in osteoarthritis

ZHIBO FAN[1-3], QIYUE FU[1-3], TAO SUN[1-3], YUTONG ZHONG[1-3], YUEFAN MA[1-3], JINGWEI JIAN[1-3], SHUOSHENG YUAN[1-3], SHENGHONG LI[1-3] and XIAOMEI XU[1-3]

[1]Department of Orthodontics, The Affiliated Stomatological Hospital of Southwest Medical University, Luzhou, Sichuan 646000, P.R. China; [2]Oral and Maxillofacial Reconstruction and Regeneration of Luzhou Key Laboratory, The Affiliated Stomatological Hospital of Southwest Medical University, Luzhou, Sichuan 646000, P.R. China; [3]Institute of Stomatology, Southwest Medical University, Luzhou, Sichuan 646000, P.R. China

Received January 23, 2026; Accepted May 4, 2026

DOI: 10.3892/ijmm.2026.5878

Abstract. Osteoarthritis (OA), characterized by articular cartilage degeneration and subchondral bone remodeling, is a notable cause of disability globally. The present study aimed to explore the role and mechanism of histone H3 lysine 18 lactylation (H3K18la) in OA osteoclast differentiation and verify the therapeutic potential of targeting this pathway. Using a mouse OA model (anterior cruciate ligament transection), RAW264.7 cell experiments, oxmacid-mediated lactate inhibition and cleavage under targets and tagmentation to map genomic targets, the present study demonstrated elevated H3K18la in OA joint osteoclasts, associated with reduced bone mineral density and aggravated subchondral bone destruction. Analysis of TRAP and lactate indicated that RANKL-induced osteoclast differentiation increased lactate production, enhancing H3K18la; oxmacid inhibited both of these processes. H3K18la was enriched at the acid phosphatase 5 promoter and directly promoted its transcription. Local oxmacid injection in OA mice decreased osteoclast numbers and alleviated subchondral bone loss. Thus, H3K18la was a key metabolic-epigenetic mediator linking glycolysis to osteoclast differentiation, representing a novel OA therapeutic target.

Introduction

Osteoarthritis (OA), a common chronic degenerative disease, affects >67 million people worldwide, creating a marked socioeconomic burden (1). Characterized by the gradual breakdown of articular cartilage and abnormal subchondral bone remodeling, OA causes painful joint symptoms, limited mobility and a notable decrease in the quality of life of patients (2).

Among the cellular contributors to OA development, osteoclasts are key mediators, regulating bone resorption by releasing acids and proteolytic enzymes, such as cathepsin K (Ctsk) (3). This activity not only damages the structural stability of the subchondral bone but also triggers cartilage destruction and joint deterioration. Previous studies have reported that inhibiting osteoclastogenesis can effectively alleviate symptoms of OA (4,5). Despite these promising results, the complex molecular mechanisms underlying osteoclast-mediated bone remodeling in OA remain incompletely understood. This presents an obstacle to developing targeted treatments, underscoring the urgent need for in-depth research into the regulatory networks that control osteoclast function in OA.

Macrophage-driven osteoclast differentiation is a highly coordinated metabolic process characterized by extensive mitochondrial biogenesis and metabolic reprogramming in response to RANKL stimulation (6). Studies have reported a marked increase in key enzymes involved in glycolysis, the tricarboxylic acid cycle and oxidative phosphorylation during osteoclastogenesis (7-9). Inhibition of lactate production or pharmacological inhibition of lactate dehydrogenase A (LDHA) suppresses osteoclast formation and alleviates OA progression in preclinical models, suggesting lactate may serve an important role in osteoclast differentiation (10-13). However, the regulatory mechanism of lactate in osteoclasts is still unclear.

Epigenetic regulation controls gene expression by altering chromatin structure, enabling cells to rapidly respond to metabolic changes. Histone modification serves a key role in this process. Lactylation, a post-translational modification (PTM) mediated by lactate, is implicated in regulating cellular functions, including macrophage polarization and immune responses (14). However, the role of lactylation in modulating osteoclastic differentiation and its potential contribution to OA remains unclear.

The present study aimed to investigate whether glycolysis and lactylation are involved in the regulation of osteoclast differentiation and to elucidate the underlying molecular

Correspondence to: Mr. Shenghong Li or Professor Xiaomei Xu, Department of Orthodontics, The Affiliated Stomatological Hospital of Southwest Medical University, No. 10, Section 2, Yunfeng Road, Jiangyang, Luzhou, Sichuan 646000, P.R. China
E-mail: lishenghong@swmu.edu.cn
E-mail: xuxiaomei@swmu.edu.cn

Key words: lactylation, histone H3 lactylation at lysine 18, osteoclast, osteoarthritis

mechanisms using *in vitro* and *in vivo* experiments, including osteoclast differentiation assays, measurement of lactate production, detection of histone lactylation levels, and analyses of gene expression and epigenetic regulation.

Materials and methods

Animal treatment. In total, 24 9-week-old male C57BL/6 mice (weight, 18-24 g) were obtained from the Animal Center of Southwest Medical University. Mice were housed under controlled conditions (temperature: 23±2˚C; humidity: 50±10%; 12/12-h light/dark cycle) with *ad libitum* access to food and water. Only male mice were used in this study to eliminate potential confounding effects of the estrous cycle and associated hormonal fluctuations on bone metabolism and osteoclast activity (15), as previously described (5). Animal health and behavior were monitored daily and body weight was recorded weekly. Humane endpoints were as follows: i) Weight loss >20% of initial body weight; ii) inability to access food or water; iii) signs of severe pain or distress (prolonged immobility, hunched posture, vocalization) unrelieved by analgesia; and iv) any condition compromising normal murine activities. No animals reached these endpoints prior to the scheduled experimental endpoint.

OA was induced via anterior cruciate ligament transection (ACLT) as described previously (5). Briefly, mice were anesthetized with isoflurane (2-3% induction, 1-2% maintenance). The right knee joint was exposed and the ACL was transected with microscissors. Sham-operated controls underwent identical exposure without ligament transection.

For model validation, 8 mice underwent the bilateral surgery, with the right knee serving as the OA model and the left knee as the sham control. A separate cohort of 16 mice all underwent ACLT surgery to establish the OA model. These mice were then randomly divided into two groups (n=8/group): OA + Vehicle group: Received daily intra-articular injections of vehicle for 2 weeks after surgery. OA + oxamic Acid group: Received daily intra-articular injections of oxamic acid for 2 weeks after surgery.

All 24 mice survived until the predefined endpoint. At 4 weeks post-surgery, mice were euthanized by CO_2 inhalation at a displacement rate of 50% chamber volume/min, followed by cervical dislocation. Death was confirmed by the absence of respiration, heartbeat and pupillary reflex. CO_2 flow was then terminated, and animals were observed for an additional 2 min prior to tissue harvest. The Animal Care and Use Committee of Southwest Medical University (Luzhou, China approved all procedures (approval no. 20241007-008), which were conducted in adherence to the ARRIVE 2.0 guidelines (16).

Micro-CT analysis. Following sacrifice, bilateral knee specimens were dissected, thoroughly cleaned of soft tissue using pre-cooled PBS and fixed in 4% paraformaldehyde at room temperature for 24 h. Samples were scanned with a high-resolution micro-CT system (SkyScan1276; Bruker Corporation) at an isotropic voxel size of 18 μm. Three-dimensional reconstruction was performed using NRecon software (version 1.7.4.2, Bruker Corporation). The subchondral bone region was analyzed for bone mineral density (BMD), trabecular thickness, trabecular separation (Tb.Sp) and bone/tissue volume ratio.

Multiplex immunohistochemistry. Knee joint specimens were fixed in 4% paraformaldehyde at room temperature for 24 h, decalcified in 10% EDTA for 14 days at room temperature, embedded in paraffin and sectioned into 4 μm slices. Sections were washed with xylene, followed by rehydration through a graded ethanol series. Antigen retrieval was performed in citrate buffer (pH 6.0) at 95-100˚C Endogenous peroxidase activity was blocked with 3% H_2O_2 for 10 min, followed by blocking with 5% BSA at room temperature (Beijing Solarbio Science & Technology Co., Ltd.; cat. no. SW3015) in TBS for 1 h. Sections were incubated overnight at 4˚C with primary antibodies against Ctsk (1:200; Proteintech Group, Inc.; cat. no. 11239-1-AP), H3K18la (1:500; Inc.; cat. no. PTM-1427RM) and L-lactyl lysine (1:200; cat. no. PTM-1401RM; both Hangzhou Jingjie Biotechnology Co., Ltd.). After PBS washing, sections were incubated with species-specific HRP-conjugated secondary antibodies (1:500; Wuhan Servicebio Technology Co., Ltd.; cat. no. GB23303) for 1 h at room temperature, followed by tyramide signal amplification using an Opal fluorophore kit (PerkinElmer, Inc.; cat. no. FP1480). Nuclei were counterstained with DAPI (Cell Signaling Technology, Inc.; cat. no. 4083) for 10 min at room temperature and slides were mounted with ProLong™ Gold Antifade reagent (Thermo Fisher Scientific, Inc.; cat. no. P36934). Images were captured with a fluorescence microscope (Olympus VS120 slide scanner, Olympus Corporation) and analyzed using ImageJ software (version 1.54p, National Institutes of Health).

Tartrate-resistant acid phosphatase (TRAP) staining. TRAP staining was performed using a commercial kit (Beijing Solarbio Science & Technology Co., Ltd.; cat. no. G1492) following the manufacturer's protocol. Briefly, sections were fixed in TRAP fixative for 1 min at room temperature, stained in TRAP substrate solution at 37˚C for 50 min and counterstained with hematoxylin for 3 min at room temperature. TRAP-positive osteoclasts (red-stained multinucleated cells) were counted using ImageJ software (version 1.54p, National Institutes of Health) and the data were presented as the number of osteoclasts/unit of bone surface area.

Safranin O/Fast green staining. Following deparaffinization and rehydration as aforementioned, 4 μm sections were stained with 0.1% Fast Green for 5 min at room temperature to visualize collagen fibers, followed by 0.1% Safranin O for 5 min at room temperature to evaluate proteoglycan content (Beijing Solarbio Science & Technology Co., Ltd.; cat. no. G1371). After dehydration in graded ethanol and xylene, the sections were mounted with Permount™ (Beijing Solarbio Science & Technology Co., Ltd.; cat. no. G8593).

Stained sections were observed under a light microscope (Olympus DP75). The images were acquired using OLYMPUS OlyVIA software (version 4.2, Olympus Corporation).

Hematoxylin and eosin staining. Following fixation, dehydration, and embedding as aforementioned, the tissue was sectioned into 4 μm sections. Tissue sections were first deparaffinized in xylene and rehydrated through a graded ethanol

Table I. Primer sequences for reverse transcription-quantitative PCR.

Gene	Sequence, 5'→3'	
	Forward	Reverse
NFATc1	CAACGCCCTGACCACCGATAG	GGCTGCCTTCCGTCTCATAGT
Ctsk	GGGAGAAAAACCTGAAGC	ATTCTGGGGACTCAGAGC
Acp5	TGTGGCCATCTTTATGCT	GTCATTTCTTTGGGGCTT
Fosl2	GTCACTCCGGGCACCTCGAAC	TTGGTCCCCGCTGCTACTGCT
β-actin	CTCCATCCTGGCCTCGCTGT	GCTGTCACCTTCACCGTTCC

NFATc1, nuclear factor of activated T cells 1; Ctsk, Cathepsin K; Acp5, tartrate-resistant acid phosphatase type 5; Fosl2, FOS-like antigen 2.

series at room temperature followed by a distilled water rinse. Nuclei were stained with Harris hematoxylin for 3-5 min at room temperature, differentiated briefly in 0.3% acid alcohol (1-2 sec at room temperature), and blued in running tap water or 0.5% lithium carbonate solution for 2-3 min at room temperature. Sections were then stained with 0.5-1% eosin for 1-3 min, dehydrated through 95 and 100% ethanol at room temperature, cleared in xylene and finally mounted with Neutral Balsam (Beyotime Biotechnology, cat. no. C0173) under a coverslip. The stained sections were observed and photographed using a light microscope (Olympus DP75).

Cell culture and treatment. RAW264.7 macrophages (China Center For Type Culture Collection; cat. no. GDC0143) were cultured in DMEM (Gibco; Thermo Fisher Scientific, Inc.) supplemented with 10% FBS (Gibco; Thermo Fisher Scientific, Inc.; cat. no. A5256701) and 1% penicillin-streptomycin and maintained at 37˚C in a 5% CO_2 incubator. For osteoclastic differentiation, cells were seeded ($1x10^4$ cells/well in 24-well plates) and treated with recombinant murine RANKL (50 ng/ml; HUABIO, cat. no. HA210876) for 0, 1, 3 or 5 days at 37˚C. To inhibit lactate production, cells were pre-treated for 24 h at 37˚C with oxmacid (0, 5, 10 or 20 mM; MedChemExpress; cat. no. HY-W013032A) (17,18) before RANKL stimulation. Lactylation induction was performed by incubating cells with sodium lactate at 37˚C (0, 5, 10 or 20 mM; MedChemExpress; cat. no. HY-W040233) for 24 h.

Cytotoxicity assay. Cell viability was assessed using the Cell Counting Kit-8 (CCK-8; APeXBIO Technology LLC; cat. no. K1018). Cells ($1x10^3$/well) were seeded in 96-well plates and treated with oxmacid (0, 5, 10, or 20 mM) at 37˚C for 24 h. Following incubation, 10 μl CCK-8 solution was added to each well and absorbance at 450 nm was measured using a microplate reader (Synergy H1, BioTek Corporation).

Reverse transcription-quantitative (RT-qPCR). Total RNA was isolated from cells using the Accurate RNA Isolation kit (Hunan Accurate Bio-Medical Technology Co., Ltd.; cat. no. AG21023), followed by RT with the Accurate RT kit (Hunan Accurate Bio-Medical Technology Co., Ltd.; cat. no. AG11705) according to the manufacturer's protocols. RT-qPCR was performed on a CFX96 Touch Real-Time PCR Detection System (Bio-Rad Laboratories, Inc.; cat. no. 185-5196) using SYBR Green Master Mix (Hunan Accurate Bio-Medical Technology Co., Ltd.). The thermocycling conditions were as follows: initial denaturation at 95˚C for 30 sec, followed by 40 cycles of 95˚C for 5 sec and 60˚C for 30 sec. Primer sequences are listed in Table I. Relative gene expression was calculated using the $2^{-\Delta\Delta Cq}$ method (19) and normalized to β-actin.

Western blot analysis. Cells were lysed on ice using RIPA buffer (Nanjing KeyGen Biotech Co.; cat. no. KGB5203-100) supplemented with protease and phosphatase inhibitors. Protein concentration was determined using a BCA assay. Equal amounts of protein (30 μg/lane) were separated by SDS-PAGE using either 10 or 12.5% polyacrylamide gels and transferred to PVDF membranes. Membranes were blocked with 5% non-fat milk in TBST containing 0.1% Tween-20 for 1 h at room temperature, then incubated overnight at 4˚C with primary antibodies against L-lactyl lysine (1:2,000; PTM BioLab, Inc.; cat. no. PTM-1427RM), histone H3 (1:2,000; HUABIO; cat. no. ET1701-64), H3K18la (all 1:2,000; PTM BioLab, Inc; cat. no. PTM-1401RM) and β-actin (1:10,000; HUABIO; cat. no. HA722023). After washing, the membranes were incubated with HRP-conjugated secondary antibodies (1:5,000; goat anti-rabbit IgG, HUABIO; cat. no. HA1012) for 1 h at room temperature. Protein bands were visualized using enhanced chemiluminescence (Affinity Biosciences; cat. no. KF8003) and images were captured using an iBright FL1500 Imaging System (Invitrogen; Thermo Fisher Scientific, Inc.; cat. no. A44241). Densitometric analysis was performed using ImageJ software (version 1.54f, National Institutes of Health). β-actin served as the loading control for non-histone proteins as it is a stable housekeeping protein with consistent expression across all experimental conditions. Total histone H3 was used for histone modifications (L-lactyl lysine, (cat. no. PTM-1427RM) and H3K18la (both Hangzhou Jingjie Biotechnology Co., Ltd.; cat. no. PTM-1401RM)) to ensure changes reflect actual levels rather than variations in total histone loading.

Immunofluorescence staining. Cells were fixed with 4% paraformaldehyde for 15 min at room temperature, permeabilized with 0.5% Triton X-100 (Beijing Solarbio Science & Technology Co., Ltd.; cat. no. IT9100) for 10 min and blocked with 5% BSA (Beijing Solarbio Science & Technology Co.,

Ltd.; cat. no. SW3015) in PBS for 1 h at room temperature. The cells were then incubated overnight at 4˚C with L-lactyl lysine and H3K18la (both 1:200) followed by a 1 h incubation at room temperature with Alexa Fluor-conjugated secondary antibodies (1:500; Abcam, cat. no. ab150084). F-actin was stained using Phalloidin-iFluor 488 (Abcam; cat. no. ab176753), and nuclei were counterstained with DAPI for 10 min at room temperature. Coverslips were mounted on glass slides using ProLong Gold Antifade reagent (Thermo Fisher Scientific, Inc.; cat. no. P36934). Images were acquired using a confocal microscope (Nikon A1 HD25, Nikon Corporation) and analyzed using ImageJ software (version 1.53t; National Institutes of Health).

Lactate and TRAP assays. Intracellular lactate levels were quantified using a Lactate Assay kit (Beijing Solarbio Science & Technology Co., Ltd.; cat. no. BC2235) according to the manufacturer's instructions. Briefly, cells were lysed and the supernatant was mixed with lactate detection reagent. Absorbance at 570 nm was measured to determine lactate production. TRAP activity was evaluated using a colorimetric kit (Beijing Solarbio Science & Technology Co., Ltd.; cat. no. BC5405) and absorbance was measured at 405 nm to assess osteoclast differentiation.

Cleavage under targets and tagmentation (CUT&Tag) library construction and sequencing. The CUT&Tag assay was performed using the Hyperactive Universal CUT&Tag Assay kit (Vazyme Biotech, cat. no. TD903-01) with modifications. Concanavalin A-coated magnetic beads ($1x10^6$ cells) were used to bind cells, followed by permeabilization with digitonin at 4˚C for 15 min. Cells were then incubated with anti-H3K18la (1:100) overnight at 4˚C. Protein A-Tn5 transposase (100 nM) was then added, and PCR amplification was conducted with Taq Plus Master Mix (Vazyme, cat. no. P218-01) as follows: initial denaturation at 95˚C for 3 min, 18 cycles of 95˚C for 30 sec, 58˚C for 30 sec, 72˚C for 30 sec and final extension at 72˚C for 5 min. The libraries were size-selected (200-600 bp) with Ampure XP beads (Beckman Coulter, cat. no. A63880) and quantified by qPCR using SYBR Green qPCR Master Mix (Vazyme, cat. no. Q711). The qPCR reaction contained universal primers targeting the Illumina adapter sequences as follows: forward, 5'-AATGATACGGCGACCACCGAGATCTACAC-3') and reverse, 5'-CAAGCAGAAGACGGCATACGAGAT-3'). The thermocycling conditions were: 95˚C for 3 min, followed by 40 cycles of 95˚C for 10 sec and 60˚C for 30 sec. For absolute quantification, a standard curve was generated using a serially diluted reference library of known concentration. The concentration of each sample library was determined by comparing its Cq value to the standard curve.

CUT&Tag data analysis. Raw reads were processed using fastp (v0.23.2; Shenzhen HaploX Biotechnology Co., Ltd.) for quality trimming and adapter removal. Clean reads were aligned to the mm10 mouse genome using Bowtie2 (v2.4.5; Johns Hopkins University). Peaks were identified using Sparse Enrichment Analysis for CUT&RUN (v1.1; Epicypher, Inc.) at a false-discovery rate <0.05 and visualized in Integrative Genomics Viewer (v 2.19.7; igv.org). Motif analysis was performed using Multiple Em for Motif Elicitation (version 5.5.3) and Discriminative Regular Expression Motif Elicitation, version 5.5.3; both from the MEME Suite). Differential peak analysis was performed using Manorm (v1.1.0; manorm.readthedocs.io/en/latest/index.html), applying a significance threshold of $P<0.05$ and $|\log2 \text{ fold-change (FC)}|>1$.

RNA sequencing (RNA-seq) and differential gene expression analysis. Total RNA was extracted using TRIzol (Thermo Fisher Scientific, Inc.). RNA integrity was verified on an Agilent 2100 Bioanalyzer (Agilent) and samples with RIN ≥7.0 were used. Libraries were prepared using the VAHTS Universal V10 RNA-seq kit (Vazyme; cat. no. NR606). The final library concentration was 10 nM. Libraries were sequenced on an Illumina NovaSeq 6000 platform using the NovaSeq 6000 S4 Reagent kit (300 cycles) (Illumina, Inc.; cat. no. 20028312), generating approximately 24 million 150-bp paired-end reads per sample.

Raw reads were processed using fastp and aligned to the mm10 genome using HISAT2 (v2.2.1; Johns Hopkins University). Gene expression was calculated by StringTie (v2.2.1; ccb.jhu.edu/software/stringtie/). Differential expression analysis was performed using DESeq2 (v1.38.3; Bioconductor). Differentially expressed genes were defined as $P<0.01$ and $|\log_2 FC| > 1$. Principal component analysis (PCA), volcano plots, WikiPathways, Gene Ontology (GO; geneontology.org/) and KEGG pathway (https://www.kegg.jp/) enrichment analyses were performed using R (v4.2.1). The WikiPathways database was accessed at https://wikipathways.org. Pathways with adjusted $P < 0.05$ were considered significantly enriched.

Chromatin immunoprecipitation (ChIP)-qPCR. ChIP assays were performed using the BeyoChIP™ Enzymatic ChIP Assay kit (Beyotime Biotechnology; cat. no. P2083S) according to the manufacturer's protocol. Briefly, chromatin from ~ $4x10^6$ cells was cross-linked with 1% formaldehyde, lysed in 100 μl of ChIP buffer, and sonicated to generate fragments of 200-1,000 bp. For each IP reaction, the lysate was incubated overnight at 4˚C with 4.8 μg of anti-H3K18la antibody (6 μg per $5x10^6$ cells) or normal rabbit IgG (Abcam; cat. no. ab133470) as a control. Immune complexes were isolated by incubation with Protein A/G Magnetic Beads. Beads were washed sequentially with low-salt, high-salt, LiCl wash buffers, and TE buffer with centrifugation at 4˚C, 12,000 x g for 1 min between each wash. Following elution and reversal of cross-links, the co-precipitated DNA was purified. Target DNA enrichment was quantified by qPCR using primers specific to the Acp5 promoter region (Table II), as aforementioned. Enrichment was calculated relative to input DNA and normalized to the IgG control.

Statistical analysis. All experiments were independently repeated at least three times and the data are presented as the mean ± standard deviation. Normality was assessed using the Shapiro-Wilk test, and homoscedasticity was verified using Levene's test. For data that followed a normal distribution and had equal variance, comparisons between two groups used the unpaired Student's t-test. One-way ANOVA with the Bonferroni post hoc correction was used for >2 group comparisons. Non-normally distributed data were analyzed using the Kruskal-Wallis test followed by Dunn's multiple comparisons test. $P<0.05$ was considered to indicate a statistically significant difference. All analyses were performed using GraphPad Prism 9.0 (Dotmatics).

Table II Primer sequences for chromatin immunoprecipitation-quantitative PCR.

Primer	Amplified region (relative to the mouse Acp5 gene TSS)	Sequence, 5'→3'	
		Forward	Reverse
Acp5-1	-1,999 to -1,415	CCGCGAGACCCTACACTTAC	ACCATCGTTCGGGTAGTTGG
Acp5-2	-1,491 to -901	TTGGCTGCCTCTCTCTCTCT	AGTTAGCGTCTCCTGGGTGA
Acp5-3	-624 to -73	TGGCAACAGGAACACGCTTA	GATGGGAGGGGATGCAAACA

TSS, transcription start site; Acp5, tartrate-resistant acid phosphatase type 5.

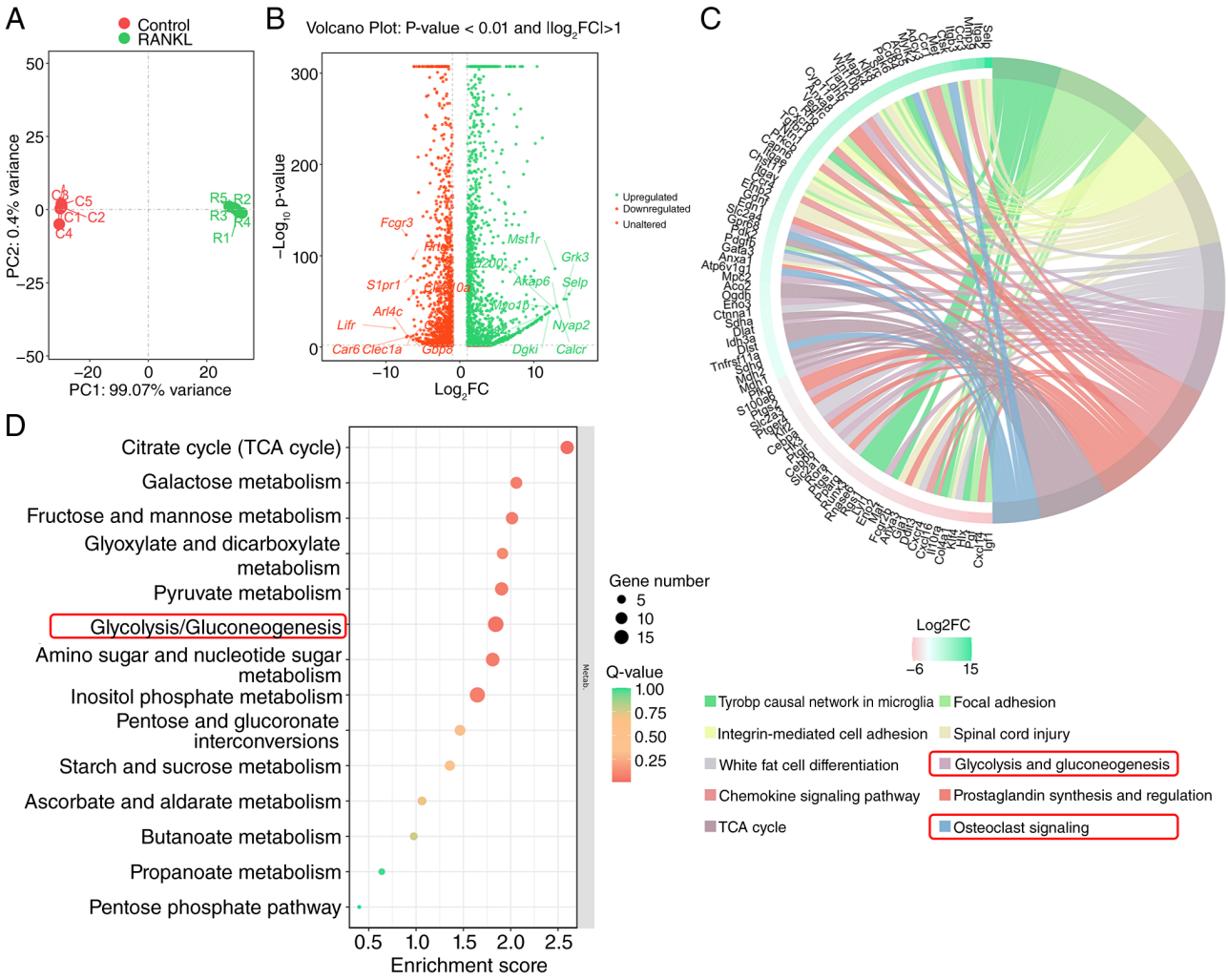

Figure 1. Analysis of the RANKL-treated and control groups based on RNA-sequencing data. (A) PCA plot. (B) Volcano plot. (C) Kyoto Encyclopedia of Genes and Genomes enrichment analysis based on the significantly differentially expressed genes (P<0.01 and |log$_2$FC| >1). (D) Bubble plot of pathway enrichment analysis (P<0.01 and |log$_2$FC| >1), focusing on carbohydrate metabolism-related pathways. (n=5). PCA, principal component analysis; KEGG; FC, fold-change.

Results

Osteoclast differentiation is accompanied by changes in carbohydrate metabolism, including the glycolysis process. To assess metabolic reprogramming during osteoclast differentiation, RNA-seq was performed on RAW264.7 macrophages with or without RANKL stimulation. PCA demonstrated clear separation between the control and RANKL-treated groups, indicating substantial transcriptomic changes during osteoclastogenesis (Fig. 1A). Differential expression analysis identified 1,496 up- and 1,321 downregulated genes (Fig. 1B).

To explore the functional implications of these transcriptional changes, KEGG pathway enrichment analysis was performed. Notably, 'glycolysis/gluconeogenesis' was among the most significantly enriched pathways, alongside 'osteoclast

signaling' (Fig. 1C and D). A chord diagram illustrated the direct association between osteoclast-associated and glycolysis pathway genes (Fig. 1C). These findings suggested that glycolytic metabolism is coupled with osteoclast differentiation, providing the rationale for investigating lactate, the end product of glycolysis, in this process.

H3K18la increases during osteoclastic differentiation. Given the enrichment of 'glycolysis/gluconeogenesis' during osteoclastogenesis, the present study evaluated whether lactate accumulation leads to histone lactylation. RAW264.7 macrophages were treated with RANKL for 0, 1, 3 or 5 days. TRAP staining revealed a progressive increase in osteoclast formation, with mature multinucleated cells appearing by day 5 (Fig. 2A and B). Concurrently, intracellular lactate levels increased in a time-dependent manner (Fig. 2D), suggesting enhanced glycolytic flux during differentiation.

Protein lactylation levels were assessed using western blotting. Pan-Kla and H3K18la signals gradually increased from day 1 to 5, paralleling the kinetics of lactate production and osteoclast maturation (Fig. 2C). LDHA, a key glycolytic enzyme, also demonstrated elevated expression. Total H3 levels remained stable across all time points, indicating that the increased H3K18la signal reflected enhanced lactylation rather than changes in histone abundance. Immunofluorescence staining revealed the nuclear accumulation of H3K18la in mature osteoclasts, with notable co-localization with F-actin rings (Fig. 2E). These findings suggested that H3K18la is dynamically upregulated during osteoclast differentiation in a lactate-dependent manner.

H3K18la is elevated in osteoclasts of OA model mice. To determine whether H3K18la levels are altered during OA pathogenesis *in vivo*, the present study established an ACLT-induced OA mouse model. Micro-CT analysis at 2 weeks post-surgery revealed notable subchondral bone loss in ACLT mice compared with that in sham-operated controls, as demonstrated by decreased BMD and increased Tb.Sp (Fig. 3A-C). Safranin O/Fast Green staining revealed cartilage degeneration and subchondral bone erosion in ACLT mice, while TRAP staining confirmed increased osteoclast numbers at the bone surface (Fig. 3A and B).

Multiplex immunofluorescence staining revealed that H3K18la signal was markedly elevated in TRAP-positive osteoclasts of ACLT mice, with a 2.3-fold increase compared with that in sham controls (Fig. 3D). Pan-Kla and Ctsk, an osteoclast marker, also revealed increased expression and co-localization. These findings indicated that H3K18la is specifically upregulated in osteoclasts under OA pathological conditions, suggesting its involvement in disease-associated bone resorption.

Inhibition of H3K18la suppresses osteoclastic differentiation. To establish the association between lactate production, H3K18la and osteoclastogenesis, RAW264.7 macrophages were treated with oxmacid, a glycolysis inhibitor that blocks lactate production (Fig. 4A). The CCK-8 assay demonstrated that oxmacid at concentrations <10 mM had no notable cytotoxicity, while 10 and 20 mM significantly decreased cell viability compared with 0 mM (Fig. 4B).

Oxmacid treatment dose-dependently decreased intracellular lactate levels (Fig. 4C) and suppressed TRAP-positive osteoclast formation (Fig. 4D and E). Moreover, western blot analysis revealed that oxmacid decreased Pan-Kla and H3K18la levels in a dose-dependent manner, while total H3 remained unchanged (Fig. 4F). LDHA expression was also reduced, consistent with glycolysis inhibition. Therefore, subsequent experiments used 10 mM oxmacid. Furthermore, immunofluorescence staining demonstrated decreased H3K18la nuclear signals in the oxmacid-treated cells (Fig. 4G). These results indicated that blocking lactate production attenuated H3K18la and inhibited osteoclast differentiation, supporting a functional role for H3K18la in this process.

Inhibition of histone lactylation alleviates OA pathology. Based on the aforementioned *in vitro* findings, the present study evaluated the therapeutic potential of targeting lactylation *in vivo*. ACLT-operated mice received intra-articular injections of oxmacid or vehicle for 2 weeks. Hematoxylin and eosin staining of major organs showed no obvious toxicity, indicating that local administration was well-tolerated (Fig. 5A).

Immunofluorescence staining revealed that oxmacid treatment significantly reduced H3K18la levels in knee joints compared with the vehicle controls (Fig. 5B). Micro-CT analysis demonstrated that oxmacid-treated mice exhibited preserved subchondral bone architecture, with higher BMD and decreased bone resorption compared with that in vehicle-treated ACLT mice (Fig. 5C). Moreover, TRAP staining revealed fewer osteoclasts in oxmacid-treated joints (Fig. 5D) and Safranin O/Fast Green staining showed attenuated cartilage degeneration compared with ACLT group (Fig. 5E). These data indicate that pharmacological inhibition of lactate production alleviated OA pathology by suppressing H3K18la-mediated osteoclast activity.

Identification of H3K18la targets during osteoclastic differentiation. To identify direct transcriptional targets of H3K18la, the present study performed CUT&Tag sequencing using H3K18la-specific antibodies in RAW264.7 macrophages in the presence or absence of RANKL stimulation. Compared with the control, H3K18la peaks were notably enriched near transcription start sites (TSS) in RANKL-treated cells, consistent with its role in transcriptional regulation (Fig. 6A). Moreover, the distribution of peaks indicated predominant localization in promoter regions (Fig. 6C).

KEGG enrichment analysis of genes associated with increased H3K18la binding identified 'osteoclast differentiation' as one of the top pathways (Fig. 6B). To refine candidate targets, the CUT&Tag data were integrated with RNA-seq data from macrophages with or without RANKL stimulation. GO enrichment analysis also showed 'osteoclast differentiation' as one of the top pathways. This combined analysis identified four osteoclast-associated genes as potential direct targets of H3K18la: Nuclear factor of activated T cells 1 (Nfatc1), Acp5, Ctsk and FOS-like antigen 2 (Fosl2; Fig. 6D and E). Among these, Acp5 demonstrated the most robust enrichment. Therefore, the present study focused on this gene for subsequent validation.

H3K18la activates Acp5 transcription. To evaluate Acp5 as a direct target of H3K18la, enriched peaks were assessed at

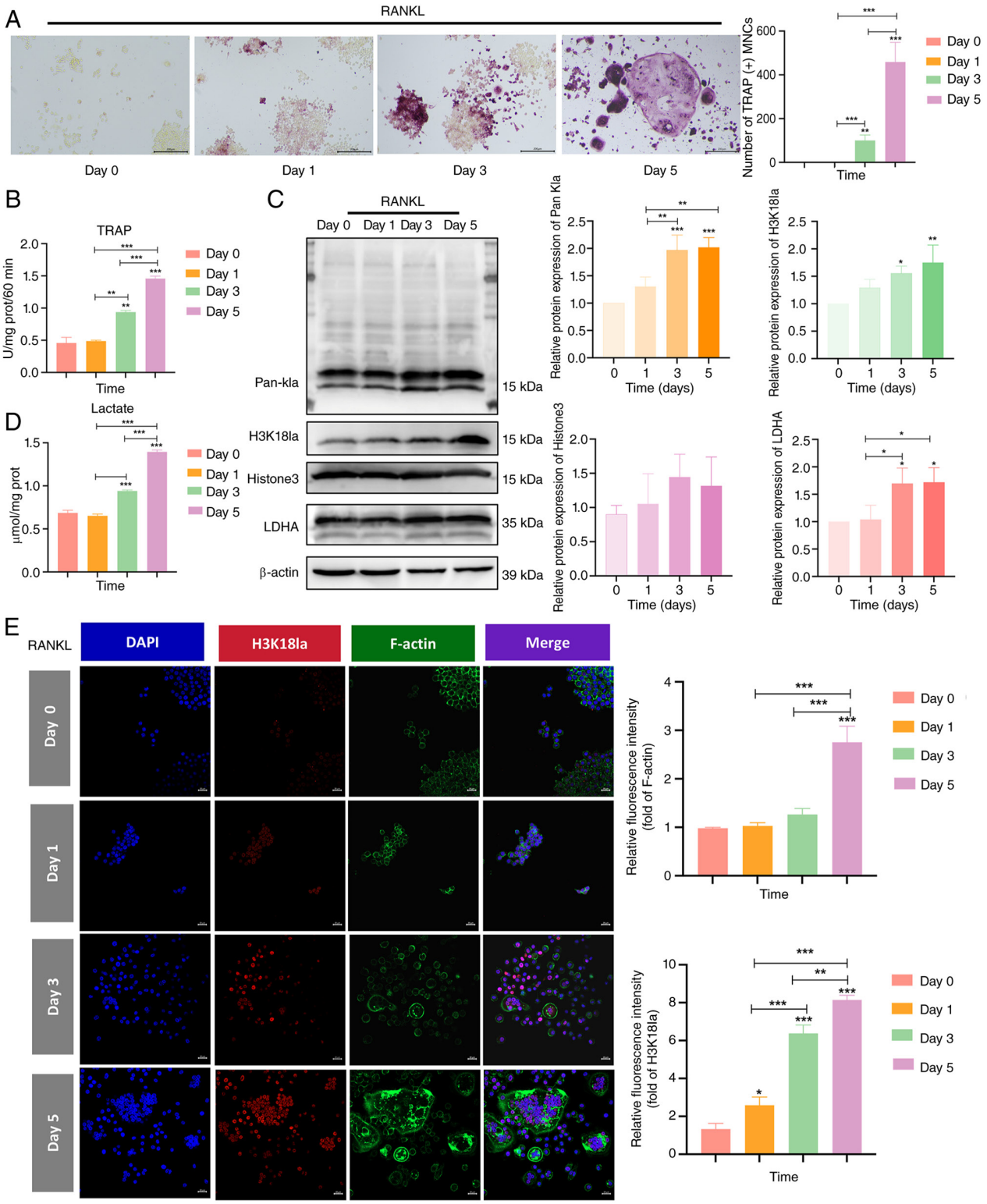

Figure 2. H3K18la increases during osteoclastic differentiation. (A) TRAP staining of macrophages following RANKL (40 ng/ml) treatment. (B) TRAP quantitative analysis of macrophages. (C) Relative protein expression of Pan-Kla, H3K18la and LDHA. (D) Lactate quantitative analysis of macrophages. (E) Immunofluorescence staining of H3K18la and F-actin protein in the knee. n=3. *P<0.05; **P<0.01; ***P<0.001 vs. day 0. H3K18la, histone H3 lactylation at lysine 18; TRAP, tartrate-resistant acid phosphatase; LDHA, lactate dehydrogenase A; Pan-Kla, pan-lysine lactylation; MNC, Multinucleated Cells; prot, protein.

the Acp5 locus. A clear H3K18la peak was observed at the Acp5 promoter region in the RANKL-treated cells, while a minimal signal was detected in controls (Fig. 7A). ChIP-qPCR was performed using three primer pairs spanning the Acp5 promoter: P1 (-1,753 to -1,177), P2 (-1,196 to -1,042) and P3 (-285 to -51). Significant H3K18la enrichment was detected at the P1 and P2 regions near the TSS, confirming direct binding at these sites (Fig. 7E).

To assess the functional consequence of this binding, macrophages were treated with exogenous lactate (10 mM) to

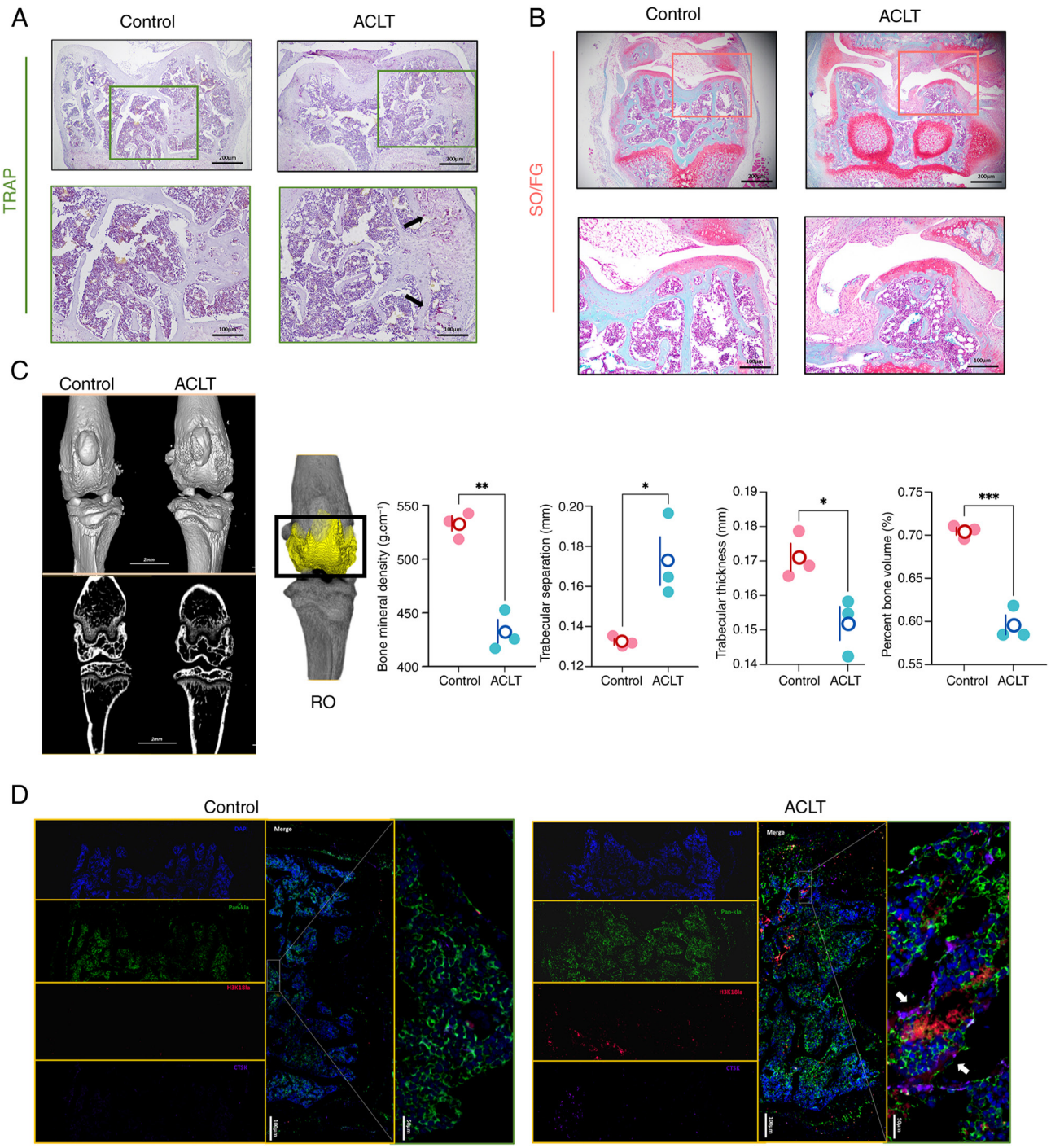

Figure 3. Elevated H3K18la in osteoclasts of OA model mice. (A) TRAP staining of the knees of mice 2 weeks after surgery. Arrows indicate osteoclasts. (B) SO/FG staining of tissue from the knee. (C) Representative micro-CT 3D images of the knee. (D) Multiple-immunofluorescence staining of Pan-kla, H3K18la and Ctsk proteins in the knee tissue. Arrows indicate areas of co-localization. n=3. *P<0.05; **P<0.01; ***P<0.001. H3K18la, histone H3 lactylation at lysine 18; OA, osteoarthritis; TRAP, tartrate-resistant acid phosphatase; SO/FG, Safranin O/fast green; Ctsk, Cathepsin K; ACLT, anterior cruciate ligament transection; ROI, region of interest.

enhance H3K18la levels. RT-qPCR revealed that compared with untreated controls, 10 mM lactate-treated significantly upregulated Acp5 mRNA expression, whilst other osteoclast markers (Nfatc1, Ctsk and Fosl2) showed no changes (Fig. 7B). Western blotting demonstrated that compared with untreated controls, 10 mM lactate increased Acp5 protein expression and elevated H3K18la (Fig. 7C). TRAP staining also revealed enhanced osteoclast formation in 10 mM lactate-treated cells, compared with untreated controls (Fig. 7D), consistent with Acp5 upregulation.

Discussion

Lactate is an important indicator of OA progression, and the gradual increase in lactate promotes the progression of OA by enhancing inflammation and degrading the cartilage matrix (17). To the best of our knowledge, however, its exact role in controlling subchondral bone destruction, a key feature of advanced OA, has not been clearly explored. The present study provided *in vivo* and *in vitro* evidence

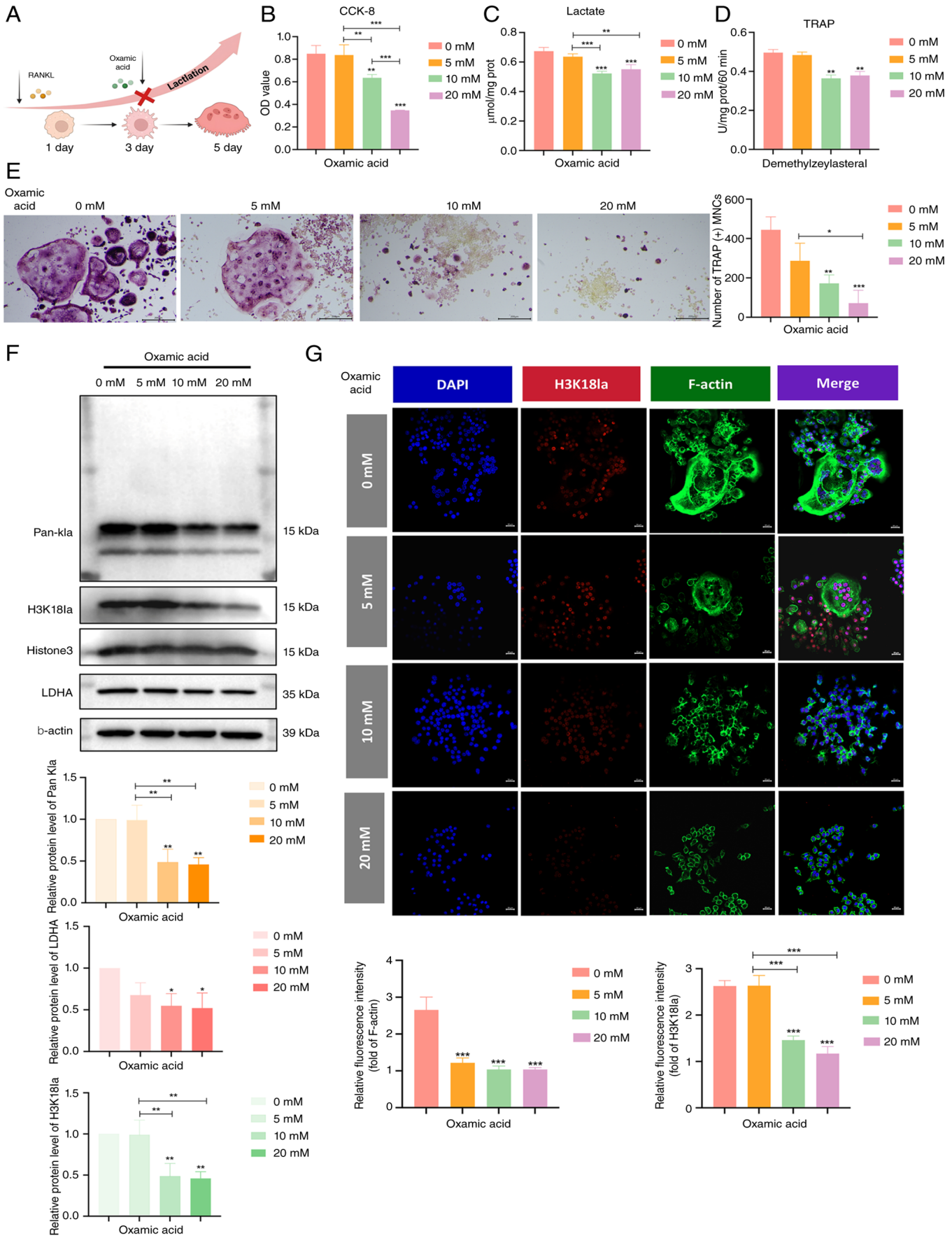

Figure 4. Inhibition of H3K18la suppresses osteoclastic differentiation. (A) Experimental inhibition of macrophage osteoclast differentiation. (B) Toxicity, (C) lactate levels and (D) TRAP-positive staining of macrophages treated with lactate inhibitors (0, 5, 10 and 20 mM). (E) TRAP staining, (F) relative protein expression of Pan-Kla, H3K18la and LDHA and (G) immunofluorescence staining of H3K18la and F-actin protein following treatment with lactate inhibitors (0, 5, 10 and 20 mM). n=3. *P<0.05; **P<0.01; ***P<0.001 vs. 0 mM. H3K18la, histone H3 lactylation at lysine 18; TRAP, tartrate-resistant acid phosphatase; Ctsk, Cathepsin K; LDHA, lactate dehydrogenase A; prot, protein; CCK-8, Cell Counting Kit-8; OD, optical density; Pan-Kla, Pan-lysine lactylation; MNC, multinucleated cells.

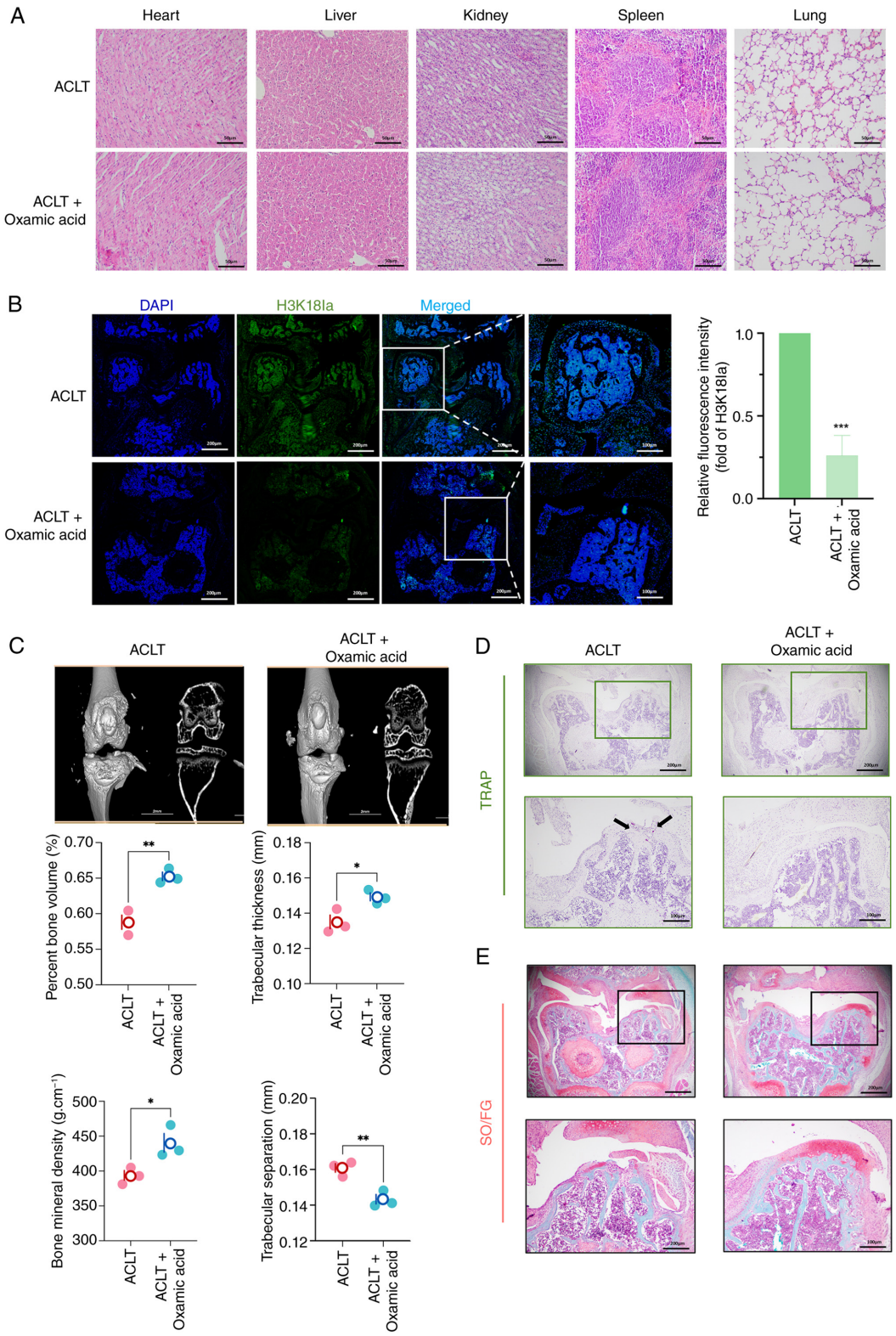

Figure 5. Inhibition of histone lactylation alleviates OA pathology. (A) Hematoxylin and eosin staining of the heart, liver, spleen, lung and kidney of mice. (B) Immunofluorescence staining of the H3K18la protein in the knee. (C) Representative micro-CT 3D of the knee. (D) TRAP staining of the knees of mice with or without lactate inhibitors. Mice received continuous local injection of oxamic acid in the knees at 2 weeks after the operation. Arrows indicate osteoclasts. (E) SO/FG staining of the knee. Black arrows indicate cartilage discontinuity; triangle indicates subchondral bone resorption. (n=3). *P<0.05; **P<0.01; ***P<0.001 vs. ACLT. OA, osteoarthritis; H3K18la, histone H3 lactylation at lysine 18; TRAP, tartrate-resistant acid phosphatase; SO/FG, Safranin O/fast green; ACLT, anterior cruciate ligament transection.

indicating that pharmacological inhibition of lactate production with oxmacid significantly decreased subchondral bone loss in an ACLT-induced mouse model of OA. This not only strengthens the association between lactate metabolism and OA progression but also reveals a previously unknown epigenetic mechanism through which lactate influences osteoclast

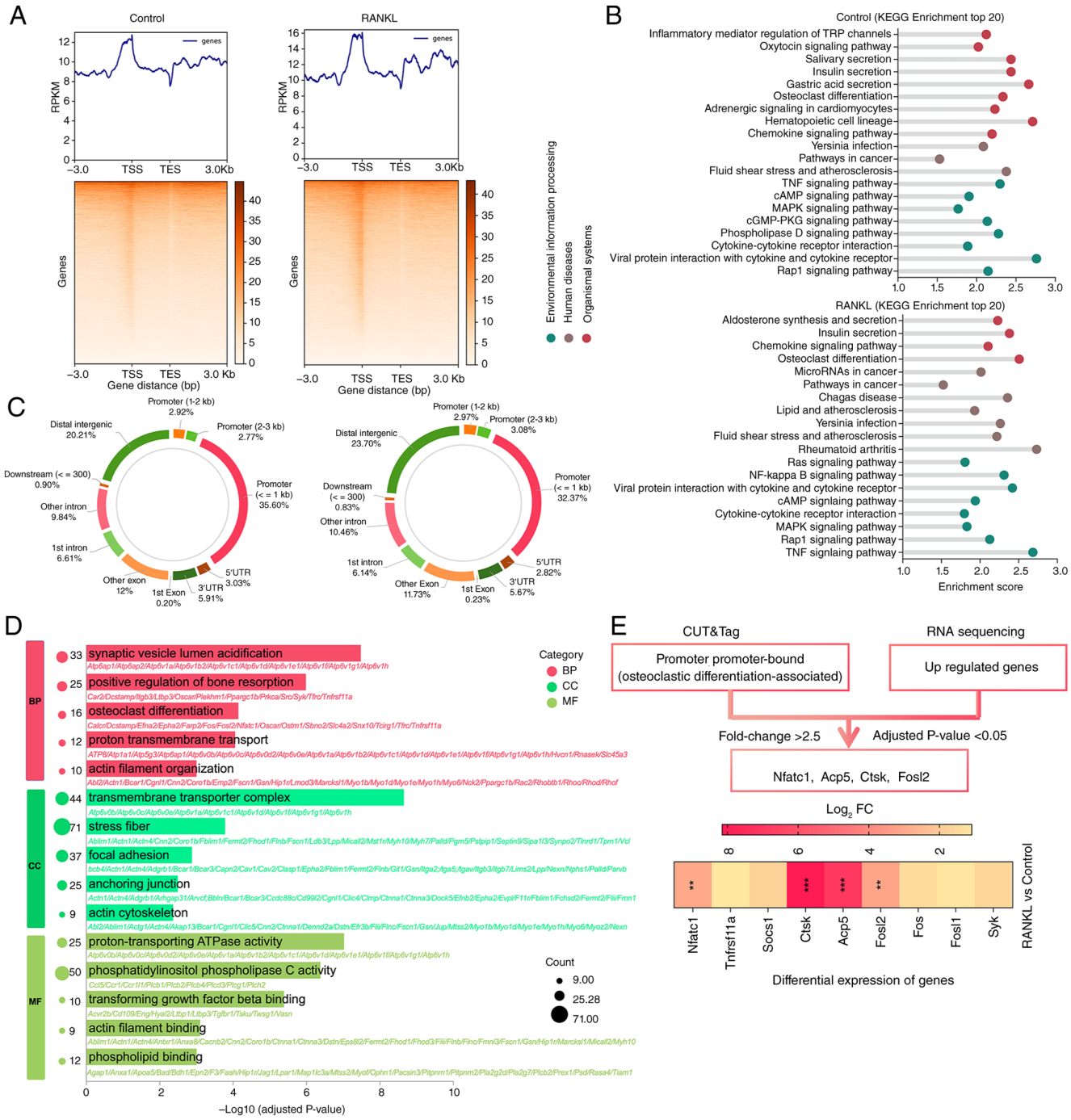

Figure 6. Identification of H3K18la targets during osteoclastic differentiation. (A) Binding density of H3K18la in macrophages with and without RANKL treatment. (B) KEGG enrichment analysis of genes with differential H3K18la binding (increased in RANKL-treated vs. control) (n=1). (C) Genome-wide distribution of H3K18la-binding peaks. (D) Gene Ontology enrichment analysis of the differentially expressed genes (P<0.01 and $|\log_2 FC| > 1$) between the two groups with RNA-seq (P<0.05; n=5). (E) CUT&Tag and scRNA-seq analyses identified upregulated targets of H3K18la (P<0.05, $|\log_2 FC| > 2.5$). **P<0.01; ***P<0.001. H3K18la, histone H3 lactylation at lysine 18; KEGG, Kyoto Encyclopedia of Genes and Genomes; FC, fold-change; scRNA-seq, single cell RNA sequencing; BP, biological process; CC, cellular component; MF, molecular function; Nfatc1, nuclear factor of activated T cells 1; Acp5, acid phosphatase 5; Ctsk, cathepsin K; RPKM, reads per kilobase of transcript per million mapped reads; Fosl2, FOS-like antigen 2.

differentiation, offering novel insights into how metabolism controls bone remodeling in OA.

Histone lactylation, a recently identified PTM, is a key regulator of gene expression in several biological processes, such as metabolic adaptation, immune response, cell death and cytoskeletal remodeling (18,20). To the best of our knowledge, the present study is the first to demonstrate a significant increase of H3K18la in osteoclasts from OA joints, which was associated with heightened osteoclast activity and faster subchondral bone resorption. This supports the glycolytic phenotype of osteoclasts, as inhibiting LDHA hampers osteoclastogenesis by disrupting energy metabolism (21-24). As lactate is the primary substrate for lactylation, it may serve as a metabolic sensor, modifying H3K18, a lysine residue located within a histone tail region that is highly responsive to metabolic changes (25,26). Using a comprehensive multi-omics

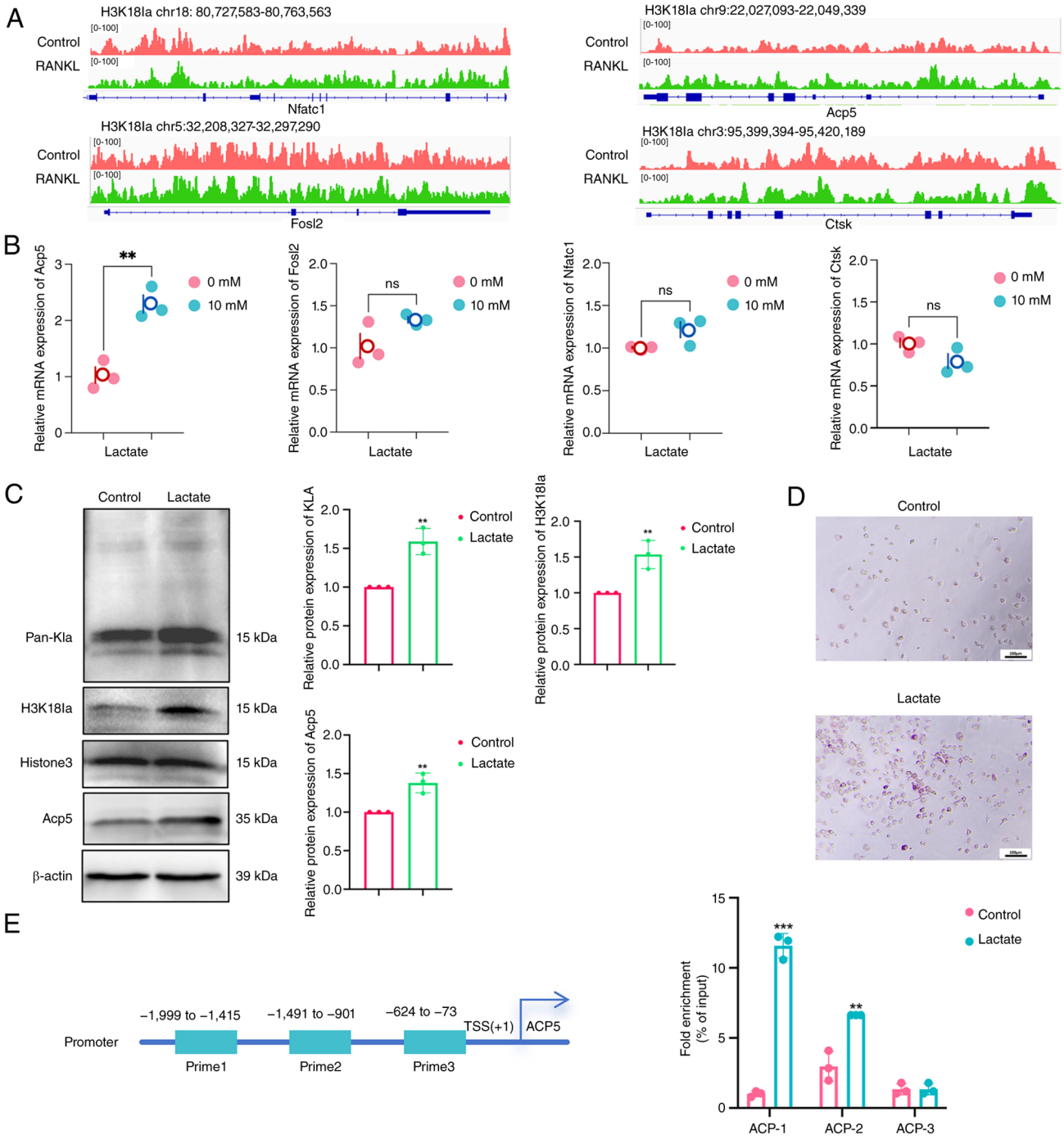

Figure 7. H3K18la activates Acp5 transcription. (A) Genome browser tracks of the CUT&Tag signal at NFATc1, Acp5, Ctsk and Fosl2. Relative (B) mRNA expression of Nfatc1, Acp5, Ctsk and Fosl2 and (C) protein expression of Pan-Kla, H3K18la and Acp5 in macrophages with or without lactate (10 mM) treatment. (D) TRAP staining of macrophages with or without lactate (10 mM) treatment. (E) H3K18la binding at the Acp5 promoter assessed by ChIP-qPCR. **P<0.01; ***P<0.001 vs. controls. H3K18la, histone H3 lactylation at lysine 18; Acp5, tartrate-resistant acid phosphatase type 5; NFATc1, nuclear factor of activated T cells 1; Ctsk, Cathepsin K; Fosl2, FOS-like antigen 2; TRAP, tartrate-resistant acid phosphatase; CHIP-q, chromatin immunoprecipitation-quantitative; Pan-Kla, Pan-lysine Lactylation; TSS, transcription start site; chr, chromosome; ns, not significant.

approach that combined CUT&Tag sequencing, ChIP-qPCR and functional experiments, the present study identified Acp5 as a direct downstream target of H3K18la. Acp5, a key enzyme that hydrolyzes phosphate esters in the bone matrix, is essential for osteoclast-driven bone resorption (27,28). The present results demonstrated a novel metabolic-epigenetic axis whereby lactate-derived lactylation of H3K18 activated Acp5 transcription, promoting osteoclast differentiation and accelerating OA progression. While the present study demonstrated the direct role for H3K18la in activating Acp5 expression, the complex interplay between histone lactylation and other PTMs, such as ubiquitination, methylation and acetylation, remains largely unexplored (25,29). These modifications typically work together to regulate gene expression during cell differentiation (30,31). H3K18la may cooperate or oppose other PTMs to regulate osteoclastogenesis and future research using advanced proteomic and epigenomic techniques is key to elucidate this complex regulatory network. Translating

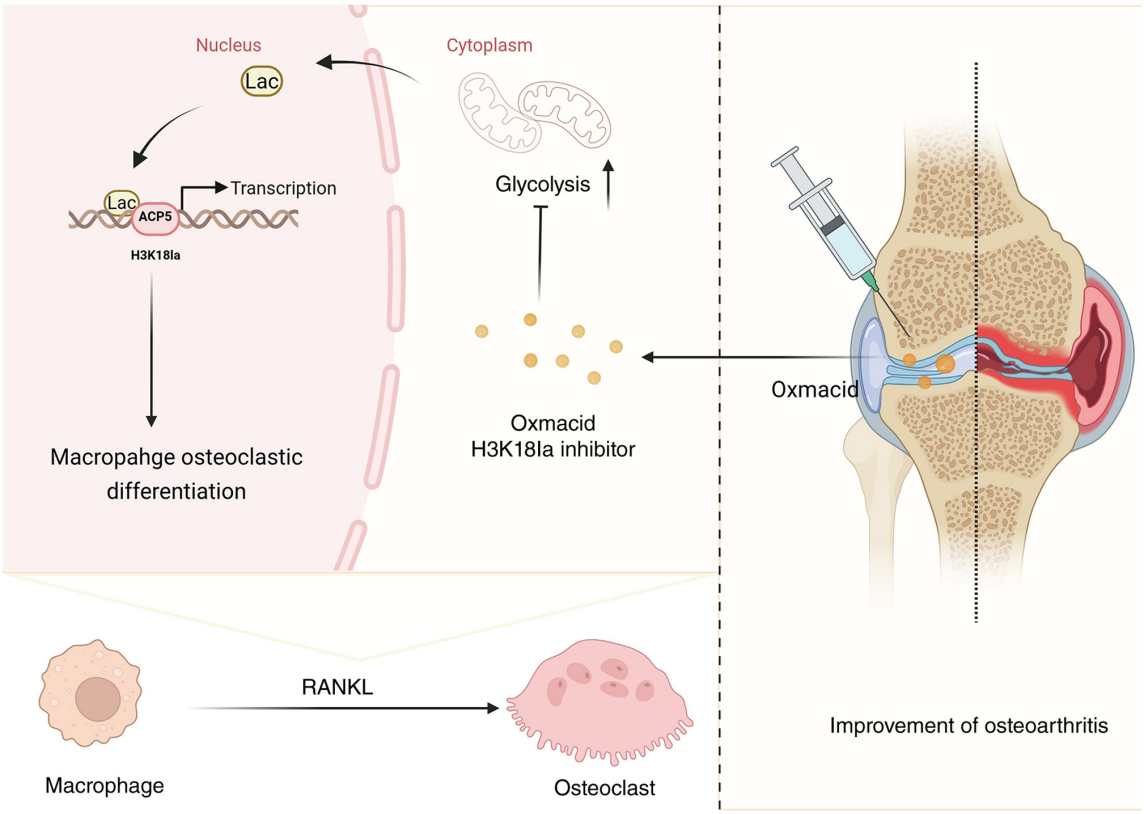

Figure 8. H3K18la affects osteoclast function by regulating Acp5 expression. Inhibition of H3K18la alleviates early bone destruction in osteoarthritis. H3K18la, histone H3 lactylation at lysine 18; Acp5, tartrate-resistant acid phosphatase type 5; Lac, lactate.

the findings of the present study to clinical settings requires validation in larger animal models and human patients. Although the preclinical data demonstrated the potential of targeting H3K18la in OA, the safety and effectiveness of lactate-lowering or lactylation-inhibiting drugs in humans need to be confirmed. Additionally, as lactate has diverse roles in different cell types within the joint environment, including chondrocytes, synovial fibroblasts and immune cells (32-35), consideration is necessary regarding potential off-target effects of such treatment.

From a broader perspective, the present study has implications for understanding the metabolic reprogramming of osteoclasts in OA. Research has highlighted the key role of cell metabolism in regulating osteoclast differentiation and function (8,36). For example, mitochondrial respiration is reported to support osteoclast maturation, while glycolysis supplies key precursors for macromolecule synthesis during this energy-intensive process (37,38). The H3K18la-Acp5 axis adds another layer of complexity to this metabolic regulation, indicating that lactate serves not only as an energy source but also as a signaling molecule to influence gene expression in osteoclasts. This may lead to new approaches for developing targeted therapies that address both metabolic dysregulation and epigenetic abnormalities in OA. However, further validation should be performed in larger animal models to avoid off-target effects caused by the pleiotropic functions of lactate. Additionally, the results of the present study have potential implications for other types of metabolic bone disease characterized by abnormal osteoclast activity, including osteoporosis and rheumatoid arthritis. Given the conserved nature of histone lactylation across different cell types and species (26), the H3K18la-Acp5 pathway may also serve a role in these diseases.

However, the present study had certain limitations. Due to the lack of specific inhibitors targeting H3K18la, inhibiting H3K18la may impact cell activities. Furthermore, in the CUT&Tag sequencing, there was only one sample/group, which may compromise the reliability. Thus, it was combined with ChIP experiments for validation to ensure the reliability of the results. Moreover, the present study only investigated H3K18la as a direct factor in osteoclastogenesis, without exploring other factors involved in the overall process of H3K18la-mediated macrophage osteoclast differentiation, such as transcription factors, metabolic regulation and epigenetic modifications. These aspects require further investigation in future studies.

In conclusion, the present study identified H3K18la as a crucial metabolic-epigenetic switch that connects glycolysis to osteoclast differentiation in OA (Fig. 8). By elucidating the molecular mechanisms underlying this new regulatory pathway, the findings offer a conceptual framework for understanding the complex association between metabolism, epigenetics and bone remodeling in OA. Although there are challenges in translating these findings into clinical practice, the present results demonstrate a promising novel target for developing disease-modifying therapy for OA and other metabolic bone disorders. Future research on the detailed regulatory networks controlling H3K18la and its downstream effectors may enhance the understanding of OA development and support the development of more effective treatment strategies.

Acknowledgements

Not applicable.

Funding

The present study was supported by the Collaborative Project of Luzhou Municipal People's Government and Southwest (grant no. 2024LZXNYDJ041) and the Project of 'Youth Scientific Research Climbing Program' of the Stomatological Hospital Affiliated to Southwest Medical University (grant no. 2024KQ05).

Availability of data and materials

The sequencing data generated in the present study may be found in the National Center for Biotechnology Information under accession number PRJNA1374074 or at the following URL: ncbi.nlm.nih.gov/bioproject/?term=%20PRJNA1374074.

Authors' contributions

ZBF and SHL confirm the authenticity of all the raw data. ZBF, SHL and XMX conceived and designed the study and wrote the manuscript. ZBF, QYF, TS, YTZ, JWJ, SSY and YFM performed the experiments and analyzed data. ZBF, QYF, TS, JWJ, YTZ, YFM, SHL and XMX reviewed and edited the manuscript. All authors have read and approved the final manuscript.

Ethics approval and consent to participate

The animal study was reviewed and approved by the Committee of Medical Experimental Animal Center of Southwest Medical University (Luzhou, China; approval no. 20241007-008).

Patient consent for publication

Not applicable.

Competing interests

The authors declare that they have no competing interests.

References

1. Zhen G, Wen C, Jia X, Li Y, Crane JL, Mears SC, Askin FB, Frassica FJ, Chang W, Yao J, *et al*: Inhibition of TGF-β signaling in mesenchymal stem cells of subchondral bone attenuates osteoarthritis. Nat Med 19: 704-712, 2013.
2. Qiu L, Alhaskawi A and Moqbel SAA: Osteoarthritis: Multitissue pathology, molecular mechanisms, clinical management, and emerging precision and regenerative therapies. Front Pharmacol 16: 1697192, 2026.
3. Jiang W, Jin Y, Zhang S, Ding Y, Huo K, Yang J, Zhao L, Nian B, Zhong TP, Lu W, *et al*: PGE2 activates EP4 in subchondral bone osteoclasts to regulate osteoarthritis. Bone Res 10: 27, 2022.
4. Ledesma-Colunga MG, Passin V, Lademann F, Hofbauer LC and Rauner M: Novel insights into osteoclast energy metabolism. Curr Osteoporos Rep 21: 660-669, 2023.
5. Zhu S, Zhu J, Zhen G, Hu Y, An S, Li Y, Zheng Q, Chen Z, Yang Y, Wan M, *et al*: Subchondral bone osteoclasts induce sensory innervation and osteoarthritis pain. J Clin Investigat 129: 1076-1093, 2019.
6. Takegahara N, Kim H and Choi Y: Unraveling the intricacies of osteoclast differentiation and maturation: Insight into novel therapeutic strategies for bone-destructive diseases. Exp Mol Med 56: 264-272, 2024.
7. Zhang D, Tang Z, Huang H, Zhou G, Cui C, Weng Y, Liu W, Kim S, Lee S, Perez-Neut M, *et al*: Metabolic regulation of gene expression by histone lactylation. Nature 574: 575-580, 2019.
8. Park-Min KH: Metabolic reprogramming in osteoclasts. Semin Immunopathol 41: 565-572, 2019.
9. Karner CM and Long F: Glucose metabolism in bone. Bone 115: 2-7, 2018.
10. Xin Q, Wang H, Li Q, Liu S, Qu K, Liu C and Zhang J: Lactylation: A passing fad or the future of posttranslational modification. Inflammation 45: 1419-1429, 2022.
11. Zhang D, Gao J, Zhu Z, Mao Q, Xu Z, Singh PK, Rimayi CC, Moreno-Yruela C, Xu S, Li G, *et al*: Lysine l-lactylation is the dominant lactylation isomer induced by glycolysis. Nat Chem Biol 21: 91-99, 2025.
12. Wang J, Yang P, Yu T, Gao M, Liu D, Zhang J, Lu C, Chen X, Zhang X and Liu Y: Lactylation of PKM2 suppresses inflammatory metabolic adaptation in Pro-inflammatory macrophages. Int J Biol Sci 18: 6210-6225, 2022.
13. Du S, Zhang X, Jia Y, Peng P, Kong Q, Jiang S, Li Y, Li C, Ding Z and Liu L: Hepatocyte HSPA12A inhibits macrophage chemotaxis and activation to attenuate liver ischemia/reperfusion injury via suppressing glycolysis-mediated HMGB1 lactylation and secretion of hepatocytes. Theranostics 13: 3856-3871, 2023.
14. Zhang H, Wang L, Cui J, Wang S, Han Y, Shao H, Wang C, Hu Y, Li X, Zhou Q, *et al*: Maintaining hypoxia environment of subchondral bone alleviates osteoarthritis progression. Sci Adv 9: eabo7868, 2023.
15. Lorenzo J: Sexual dimorphism in osteoclasts. Cells 9: 2086, 2020.
16. Percie Du Sert N, Ahluwalia A, Alam S, Avey MT, Baker M, Browne WJ, Clark A, Cuthill IC, Dirnagl U, Emerson M, *et al*: Reporting animal research: Explanation and elaboration for the ARRIVE guidelines 2.0. PLoS Biol 18: e3000411, 2020.
17. Yang J, Li W, Lin X and Liang W: A lactate metabolism-related gene signature to diagnose osteoarthritis based on machine learning combined with experimental validation. Aging (Albany NY) 16: 13076-13103, 2024.
18. Xia J, Qiao Z, Hao X and Zhang Y: LDHA-induced histone lactylation mediates the development of osteoarthritis through regulating the transcription activity of TPI1 gene. Autoimmunity 57: 2384889, 2024.
19. Livak KJ and Schmittgen TD: Analysis of relative gene expression data using real-time quantitative PCR and the 2(-Delta Delta C(T)) method. Methods 25: 402-408, 2001.
20. Huang YF, Wang G, Ding L, Bai ZR, Leng Y, Tian JW, Zhang JZ, Li YQ, Ahmad, Qin YH, *et al*: Lactate-upregulated NADPH-dependent NOX4 expression via HCAR1/PI3K pathway contributes to ROS-induced osteoarthritis chondrocyte damage. Redox Biology 67: 102867, 2023.
21. Wang J, Guan H, Liu H, Lei Z, Kang H, Guo Q, Dong Y, Liu H, Sun Y, Fang Z and Li F: Inhibition of PFKFB3 suppresses osteoclastogenesis and prevents ovariectomy□induced bone loss. J Cell Mol Med 24: 2294-2307, 2020.
22. Hu W, Chen Y, Dou C and Dong S: Microenvironment in subchondral bone: Predominant regulator for the treatment of osteoarthritis. Ann Rheum Dis 80: 413-422, 2021.
23. Li B, Lee W, Song C, Ye L, Abel ED and Long F: Both aerobic glycolysis and mitochondrial respiration are required for osteoclast differentiation. FASEB J 34: 11058-11067, 2020.
24. Nishioku T, Anzai R, Hiramatsu S, Terazono A, Nakao M and Moriyama M: Lactate dehydrogenase A inhibition prevents RANKL-induced osteoclastogenesis by reducing enhanced glycolysis. J Pharmacol Sci 153: 197-207, 2023.
25. Peng X and Du J: Histone and non-histone lactylation: Molecular mechanisms, biological functions, diseases, and therapeutic targets. Mol Biomed 6: 38, 2025.
26. Galle E, Wong CW, Ghosh A, Desgeorges T, Melrose K, Hinte LC, Castellano-Castillo D, Engl M, de Sousa JA, Ruiz-Ojeda FJ, *et al*: H3K18 lactylation marks tissue-specific active enhancers. Genome Biol 23: 207, 2022.
27. Rathod B, Desai S, Samvelyan HJ, Bock L, Wu J, Ohlsson C, Palmquist A, Alm JJ, Newton PT, Andersson G and Windahl SH: Tartrate-resistant acid phosphatase (TRAP/ACP5) promotes bone length, regulates cortical and trabecular bone mass, and maintains growth plate architecture and width in a sex- and site-specific manner in mice. Bone 188: 117223, 2024.

28. Ivanova MM, Dao J, Loynab N, Noor S, Kasaci N, Friedman A and Goker-Alpan O: The expression and secretion profile of TRAP5 isoforms in gaucher disease. Cells 13: 716, 2024.
29. Shen Y, Mao Z, Chen H, Zhu W, Guan Q, Yang Y, Liu J and Li L: Exercise-specific post-translational modification signatures: Unveiling precise regulatory mechanisms of molecular exercise language and cellular adaptation. Front Sports Act Living 8: 1765170, 2026.
30. Balsalobre A and Drouin J: Pioneer factors as master regulators of the epigenome and cell fate. Nat Rev Mol Cell Biol 23: 449-464, 2022.
31. Chisolm DA and Weinmann AS: Connections between metabolism and epigenetics in programming cellular differentiation. Annu Rev Immunol 36: 221-246, 2018.
32. Zheng J, Lu Y, Lin Y, Si S, Guo B, Zhao X and Cui L: Epitranscriptomic modifications in mesenchymal stem cell differentiation: Advances, mechanistic insights, and beyond. Cell Death Differ 31: 9-27, 2024.
33. Cheung KC, Ma J, Wang L, Chen X, Fanti S, Li M, Azevedo LR, Gosselet F, Shen H, Zheng X, *et al*: CD31 orchestrates metabolic regulation in autophagy pathways of rheumatoid arthritis. Pharmacol Res 207: 107346, 2024.
34. Zhu Z, Chen Y, Zou J, Gao S, Wu D, Li X, Hu N, Zhao J, Huang W and Chen H: Lactate mediates the bone anabolic effect of High-intensity interval training by inducing osteoblast differentiation. J Bone Joint Surg Am 105: 369-379, 2023.
35. Pucino V, Nefla M, Gauthier V, Alsaleh G, Clayton SA, Marshall J, Filer A, Clark AR, Raza K and Buckley CD: Differential effect of lactate on synovial fibroblast and macrophage effector functions. Front Immunol 14: 1183825, 2023.
36. Da W, Tao L and Zhu Y: The role of osteoclast energy metabolism in the occurrence and development of osteoporosis. Front Endocrinol (Lausanne) 12: 675385, 2021.
37. Estell E, Ichikawa T, Giffault P, Bonewald L, Spiegelman B and Rosen C: Irisin enhances mitochondrial function in osteoclast progenitors during differentiation. Biomedicines 11: 3311, 2023.
38. Chen L, Su Y, Wang C, Huang Q, Chen W, Hai N, Wang J, Lian H, Zhao J, Xu J and Liu O: Rc3h1 negatively regulates osteoclastogenesis by limiting energy metabolism. Theranostics 14: 7554-7568, 2024.